The Astrophysical Journal, 621:738–749, 2005 March 10
© 2005. The American Astronomical Society. All rights reserved. Printed in U.S.A.

THE CORE OF NGC 6240 FROM KECK ADAPTIVE OPTICS AND *HUBBLE SPACE TELESCOPE* NICMOS OBSERVATIONS

C. E. Max,[1] G. Canalizo,[2] B. A. Macintosh,[3] L. Raschke,[4] D. Whysong,[5] R. Antonucci,[5] and G. Schneider[6]

Received 2004 June 28; accepted 2004 November 10

ABSTRACT

We present results of near-infrared imaging of the disk-galaxy merger NGC 6240 using adaptive optics on the Keck II telescope and reprocessed archival data from NICMOS on the *Hubble Space Telescope*. Both the northern and southern nuclei of NGC 6240 are clearly elongated, with considerable substructure within each nucleus. In K' band there are at least two point sources within the northern nucleus; we tentatively identify the southwestern point source within the northern nucleus as the position of one of the two active galactic nuclei (AGNs). Within the southern nucleus, the northern subnucleus is more highly reddened. Based on the nuclear separation measured at 5 GHz, we suggest that the AGN in the southern nucleus is still enshrouded in dust at K' band and is located slightly to the north of the brightest point in K' band. Within the southern nucleus there is strong H_2 1–0 $S(1)$ line emission from the northern subnucleus, contrary to the conclusions of previous seeing-limited observations. Narrowband H_2 emission line images show that a streamer or ribbon of excited molecular hydrogen connects the northern and southern nuclei. We suggest that this linear feature corresponds to a bridge of gas connecting the two nuclei, as seen in computer simulations of mergers. Many pointlike regions are seen around the two nuclei. These are most prominent at 1.1 μm with NICMOS and in K' band with Keck adaptive optics. We suggest that these point sources represent young star clusters formed in the course of the merger.

Subject headings: galaxies: active — galaxies: individual (NGC 6240) — galaxies: interactions — instrumentation: adaptive optics

1. INTRODUCTION

Mergers and interactions of gas-rich galaxies are thought to be important triggers for both nuclear activity and starbursts (e.g., Kennicutt & Keel 1984; Norman & Scoville 1988; Sanders & Mirabel 1996; Barnes & Hernquist 1996; Genzel et al. 1998). Indeed the resulting starbursts and active galactic nuclei (AGNs) may well be causally related. Winds and outflows from starbursts can provide fuel to "feed" the central black hole of the AGNs (e.g., Canalizo & Stockton 2001), and gravitational torques can remove angular momentum from shocked galactic gas (Barnes & Hernquist 1991, 1996), allowing the gas to fall in toward the black hole and fuel it.

NGC 6240 ($z = 0.0243$, $d = 98$ Mpc for $H_0 = 75$ km s^{-1} Mpc^{-1}, $1'' = 470$ pc) is a merger of two massive disk galaxies (Fosbury & Wall 1979; Tacconi et al. 1999). It contains two nuclei separated by 1.″5–1.″7 (see, e.g., optical images in Gerssen et al. 2004; Rafanelli et al. 1997; near-IR images in Scoville et al. 2000; radio images in Beswick et al. 2001; Gallimore & Beswick 2004). In the optical through infrared, the angular separation between the two nuclei is known to decrease toward longer observing wavelength, suggesting heavy dust extinction in the nuclear regions. On larger spatial scales, the optical emission of NGC 6240 shows a dramatic "bow tie" structure with tidal tails of the type seen in computer simulations of merging disk galaxies (e.g., Toomre & Toomre 1972) and observed in many other galaxy mergers. NGC 6240 has been known from X-ray observations by *BeppoSAX* (Vignati et al. 1999) and *ASCA* (Iwasawa & Comastri 1998) to contain at least one AGN, highly absorbed at X-ray wavelengths. In 2002 November it was announced (Komossa et al. 2003) that *Chandra* high-energy X-ray observations using the ACIS-S detector have resolved two AGNs, one in each nucleus, with approximately the same separation as the two compact nuclei seen at 5 GHz by MERLIN (Gallimore & Beswick 2004). Visible-light spectroscopy classifies NGC 6240 as a LINER (Veilleux et al. 1995).

Infrared observations of NGC 6240 by *IRAS* (Wright et al. 1984) and the *Infrared Space Observatory* (*ISO*; Genzel et al. 1998; Lutz et al. 2003) classify it as a luminous infrared galaxy (LIRG) and show that NGC 6240 contains an ongoing starburst. Indeed its infrared luminosity $L_{IR} \sim 10^{12}\ L_\odot$ places it on the boundary between LIRGs and their bigger brothers, ultraluminous infrared galaxies (ULIRGs). Physical conditions pertaining to the starburst activity (both gas and stars) have been under active investigation via infrared spectroscopy (e.g., Tecza et al. 2000; Ohyama et al. 2000, 2003; Lutz et al. 2003), as well as via radio and millimeter-wave interferometry (e.g., Beswick et al. 2001; Gallimore & Beswick 2004; Tacconi et al. 1999). A superwind is seen in Hα emission (Heckman et al. 1987, 1990; Armus et al. 1990) and in H_2 line emission (Wright et al. 1984; Joseph et al. 1984), presumably driven by the starburst activity. At infrared wavelengths, NGC 6240 has the most powerful galactic H_2 line emission known to date: $L(H_2) \sim 2 \times 10^9\ L_\odot$ (Joseph et al. 1984).

[1] Center for Adaptive Optics, University of California, 1156 High Street, Santa Cruz, CA 95064; and Institute of Geophysics and Planetary Physics, Lawrence Livermore National Laboratory, 7000 East Avenue, Livermore, CA 94550; max@ucolick.org, max1@llnl.gov.

[2] Current address: Department of Earth Sciences and Institute of Geophysics and Planetary Physics, University of California, Riverside, CA 92521; gabriela.canalizo@ucr.edu.

[3] I Division, Lawrence Livermore National Laboratory, 7000 East Avenue, Livermore, CA 94550; bmac@igpp.ucllnl.org.

[4] Center for Adaptive Optics, University of California, 1156 High Street, Santa Cruz, CA 95064; lynne@ucolick.org.

[5] Physics Department, University of California, Broida Hall, Building 572, Santa Barbara, CA 93106; ski@spot.physics.ucsb.edu, dwhysong@physics.ucsb.edu.

[6] Steward Observatory, University of Arizona, 933 North Cherry Avenue, Tucson, AZ 85721; gschneider@stsci.edu.

Because of the relative proximity of NGC 6240, the physical relationship between its stellar populations and gas can now be studied at high spatial resolution. Here 1″ corresponds to 470 pc, so that scales of ∼25 pc have been probed using visible-light (Rafanelli et al. 1997; Gerssen et al. 2001, 2004) observations with the *Hubble Space Telescope* (*HST*). Scales of ∼50 pc are probed using adaptive optics (AO) on 8–10 m telescopes and using the NICMOS camera on *HST*, as reported here and by Scoville et al. (2000). Near-infrared continuum emission in the nuclear regions arises from a combination of stellar continuum and warm dust. H_2 line emission arises when molecular hydrogen gas is excited by shocks or by hard photons; both excitation sources can be produced, in principle, by either the starburst or the AGNs.

In this paper we use high spatial resolution observations in the near-infrared from both Keck Telescope AO and NICMOS with the *Hubble Space Telescope* to address the following pieces of the puzzle of how the two AGNs, the merger event, and the starburst activity are related:

1. Geometry, extinction, and relative positions of the two nuclei: What is the infrared morphology of the two nuclei? What is the relation between nuclear features seen in the near-infrared and those in the optical? Which features in the near-infrared and optical correspond to the radio and hard X-ray point sources?
2. Geometry for the excited gas and winds: What is the relationship between the Hα-emitting gas and the H_2-emitting gas? Does the excited molecular hydrogen seen in the near-infrared relate to the dense concentration of CO observed by Tacconi et al. (1999) between the two nuclei? How do the observed regions of excited H_2- and Hα-emitting gas fit into the scenario in which "bubbles" of hot gas seen in low-energy X-rays (Komossa et al. 2003) occupy the regions surrounding the double nucleus?

2. TELESCOPES AND INSTRUMENTS

2.1. *Keck Telescope*

The Keck II AO system (Wizinowich et al. 2000a, 2000b; Johansson et al. 2000) is located on an optical bench at the Nasmyth platform of the 10 m Keck II telescope. The Xinetics deformable mirror has 349 degrees of freedom, of which approximately 249 are illuminated at any given time as the hexagonal pupil of the telescope rotates on the round deformable mirror. The Shack-Hartmann wavefront sensor is based on a 64×64 pixel Lincoln Laboratories CCD with read noise of approximately 6 electrons pixel^{-1}. The real-time computer is based on the Mercury RACE architecture and uses 16 Intel i860 floating-point CPUs.

For the observations reported here, the wavefront sensor's sample rate was 90–100 Hz on a guide star of magnitude $R = 11.9$, $B = 13.5$, located at a distance of 35.″8 from the midpoint between the dual nuclei; for these parameters the control system's closed-loop bandwidth was typically 5–10 Hz. The measured Strehl ratio of the guide star itself was ∼45% when these observations were taken. We could not measure the Strehl ratio at the position of NGC 6240's dual nuclei because the wings of the point-spread functions (PSFs) of the numerous pointlike sources in the nucleus are lost in the general diffuse light from the two galaxies. If we use the theory of (infinite aperture) anisoplanatism assuming Kolmogorov turbulence and estimate the Mauna Kea *K*-band isoplanatic angle as $\theta_0 \sim 30''$, then we would estimate the Strehl ratio at the nucleus of NGC 6240, 35.″8 from the guide star, as $S_{\rm nuc}/S_{\rm gs} = \exp - (\theta/\theta_0)^{5/3}$ or $S_{\rm nuc} \sim$ 10%. Without the benefit of a real-time PSF estimator for Shack-Hartmann sensing that is analogous to that developed by Véran for curvature sensing (Véran et al. 1997) we do not have a direct measurement of the off-axis Strehl ratio.

The NIRC-2 instrument that we used at Keck (PI: K. Matthews) is a near-infrared camera providing high-resolution imaging in conjunction with the AO system on the Keck II telescope. The instrument features a Boeing 1024×1024 Aladdin-3 InSb detector array. Three cameras are available, providing fields of view measuring 10″, 20″, and 40″ on a side, with nominal plate scales of 0.″01, 0.″02, and 0.″04 pixel^{-1}, respectively. These correspond to Nyquist sampling the diffraction-limited FWHM for imaging at 1, 2, and 4 μm. For the work reported here we used the "wide" camera (40″ field of view, 0.″039686 pixel^{-1}). NIRC2 also provides diffraction-limited grism spectroscopy, which we will report on elsewhere.

2.2. *Hubble Space Telescope*

On *HST*, the NICMOS camera employs NICMOS3/PACE 256×256 HgCdTe detectors, which in Camera 2 (its "intermediate" field camera, $19.''2 \times 19.''3$) samples the f/45 reimaged 2.4 m primary mirror focal plane at a scale of 0.″076 pixel^{-1}. See Thompson et al. (1998) and Roye et al. (2003) for details of the NICMOS instrument and its performance on *HST*. The spacecraft can be repointed with high precision, enabling very fine subpixel dithers (to <0.1 pixel precision in Camera 2) to better sample the *HST* plus instrumental PSF.

3. OBSERVATIONS

Table 1 summarizes our Keck AO imaging observations. A natural guide star was used as the wavefront reference source. This star, with coordinates $16^{\rm h}53^{\rm m}01^{\rm s}.218$, $+02^\circ24'14''.49$ (J2000.0), has magnitude $R = 11.9$, $B = 13.5$, and is 35.″8 away from the midpoint between the two nuclei of NGC 6240. With NIRC2, we observed the NGC 6240's double nucleus in three broadband filters, K' (central wavelength $\lambda_c = 2.124$ μm, FWHM $\Delta\lambda = 0.351$ μm), H ($\lambda_c = 1.633$ μm, $\Delta\lambda = 0.2146$ μm), and J ($\lambda_c = 1.248$ μm, $\Delta\lambda = 0.163$ μm), and two narrowband filters, nominal Brγ ($\lambda_c = 2.1642$ μm, $\Delta\lambda = 0.0339$ μm) and nominal H_2 (called NB2108 on the Keck Web site; $\lambda_c = 2.1244$ μm, $\Delta\lambda = 0.0321$ μm). The filter transmission functions for the Keck Brγ and H_2 filters are shown in Figure 1*a*. These two filters were chosen because the strongest observed lines of H_2 seen in our spectra of the two nuclei and the region between them fall within the bandpass of the nominal Brγ filter, whereas the adjacent short-wavelength continuum falls within the bandpass of the nominal H_2 filter.

Table 2 summarizes the raw NICMOS data that we acquired from the *HST* archive. The NICMOS images reported on in this paper were obtained by recalibrating and reprocessing these archival data. Wide-band F110W ($\lambda_c = 1.100$ μm, FWHM = 0.592 μm; roughly analogous to *J* band), F160W ($\lambda_c = 1.594$ μm, FWHM = 0.403 μm; similar to *H* band), and

TABLE 1
KECK ADAPTIVE OPTICS OBSERVATIONS OF NGC 6240

Date (UT)	Filter	Integration Time (s)
2002 Aug 4	Brγ	1200
	NB2108	1200
2003 Aug 17	*J*	300
	H	270
	K′	390

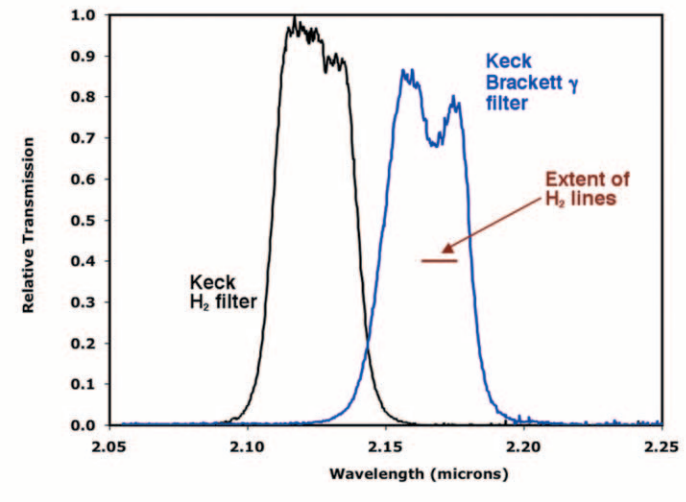

FIG. 1*a*

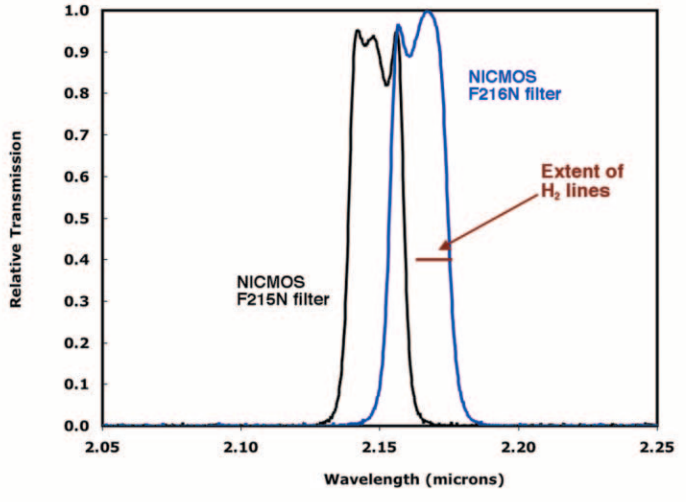

FIG. 1*b*

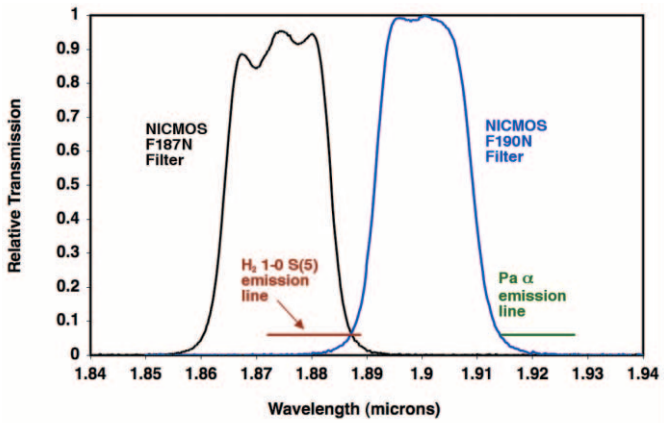

FIG. 1*c*

FIG. 1.—Narrowband filters. (*a*) Bandpass plots of Brγ and H_2 (NB2108) filters for the NIRC2 AO camera at the Keck II telescope. The H_2 1–0 $S(1)$ line of NGC 6240 falls entirely within the Brγ filter, as shown by the red horizontal bar. (*b*) Bandpass plots of NICMOS F215N and F216N filters. The H_2 1–0 $S(1)$ line of NGC 6240 falls entirely within the F216N filter. (*c*) Bandpass plots of NICMOS F187N and F190N filters. The H_2 1–0 $S(5)$ line of NGC 6240 falls largely within the high-sensitivity portion of the F187N filter. The Paα line is redshifted largely, but not entirely, out of the F190N filter. In these figures the widths of the red horizontal bars (H_2 lines) were estimated from spectra (reported elsewhere). The width of the Paα line (panel [*c*]) was estimated from that of the Brγ line seen in our spectra.

F222M ($\lambda_c = 2.216$ μm, FWHM $= 0.143$ μm; similar to K' band) images of NGC 6240 were obtained as part of GTO program 7219 (PI: Scoville) using the NIC2 camera, on 1998 February 2 in a single *HST* orbit. NICMOS narrowband images in the 1–0 $S(1)$ transition of molecular hydrogen used the NIC2 camera with the F216N ($\lambda_c = 2.149$ μm, FWHM $= 0.020$ μm) and F215N ($\lambda_c = 2.164$ μm, FWHM $= 0.021$ μm) filters, GO program 7882 (PI: van der Werf) acquired 1998 March 3–4.

TABLE 2

HST NICMOS OBSERVATIONS OF NGC 6240 DISCUSSED HERE

Observing Program	Filter	Camera	Integration Time (s)
GTO 7219 (PI: Scoville)	F222M	NIC2	224
	F160W	NIC2	192
	F110W	NIC2	160
	F187N	NIC2	218
	F190N	NIC2	218
GO 7882 (PI: van der Welf).....	F216N	NIC2	4096
	F215N	NIC2	3072

The NICMOS F215N and F216N filters are narrower than their Brγ and H_2 narrowband counterparts at Keck (compare Figs. 1*a* and 1*b*), but for the present purposes this makes no difference because our spectra (to be described elsewhere) show that emission lines in the nuclei of NGC 6240 are confined to the NICMOS F216N and Keck Brγ filters, as shown by the red lines in Figures 1*a* and 1*b*.

NICMOS GTO program 7219 also observed NGC 6240 in a pair of narrowband filters usually used for Paα (rest wavelength 1.875 μm), whose bandpasses are shown in Figure 1*c*. At the redshift of NGC 6240 ($z = 0.0243$) the Paα line is shifted almost out of the F190N filter, as shown by the green line in Figure 1*c*. The 1–0 $S(5)$ transition of molecular hydrogen (rest wavelength 1.8358 μm) is redshifted squarely into the F187N filter. Thus, the difference between the F187N (emission line) and F190N (continuum) filters gives an image of the core of NGC 6240 in the H_2 1–0 $S(5)$ transition. However, because the Paα line can be quite strong in galaxies such as NGC 6240, we cannot completely discount its potential contribution to the difference between the fluxes in F187N and F190N. Although the flux difference is dominated by the 1–0 $S(5)$ line of H_2, we have chosen not to perform relative photometry between this

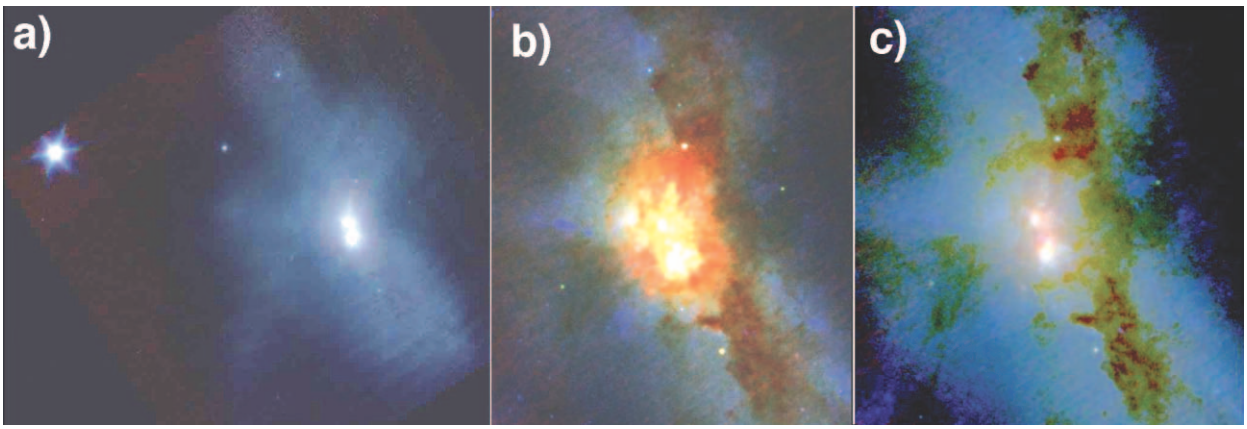

FIG. 2.—Multiwavelength images of NGC 6240. North is up and east is to the left in all figures in this paper. (*a*) False-color wide-field image of NGC 6240, with Keck AO. K' band is represented by red, H band by green, and J band by blue. The (overexposed) guide star is on the far left of this image and is about 36″ from the double nucleus. This image is 59″ wide by 47″ tall. The large-scale shape of the galaxy as seen in J-band light is similar to the bow tie shape long known in the visible (see Fig. 2 in Pasquali et al. 2003). (*b*) False-color image of NGC 6240 over a narrower field (28.″5 × 33″) than in (*a*) as seen by the WFPC2 PC chip on *HST* and with Keck AO. This is a linear color map; red represents K' band from Keck AO, green is the F814W filter from WFPC2 on *HST*, and blue is the F450W filter from WFPC2 on *HST*. The large dust lanes in (or in front of) the nuclear area are clearly seen. (*c*) Same as (*b*), but a logarithmic color map so that the double nuclei are not saturated.

narrowband filter pair and the F215N/F216N pair on account of the modest but unknown contribution of Paα.

4. DATA ANALYSIS TECHNIQUES

The NIRC2 data were reduced using standard techniques for near-infrared imaging. Bad pixels were masked out when combining the dithered images to obtain a final image. Flat fields were constructed from twilight exposures at each filter bandpass. Dark frames were created for each exposure time. Each dithered image was sky-subtracted, dark-subtracted, and flat-fielded. Deconvolution was not used for the images discussed in this paper.

NICMOS broadband images were reduced as follows. All data were taken in STEP8 multiaccum sequences: F110W with NSAMP = 10 (40 s integrations), F160W with NSAMP = 11 (48 s integrations), and F222M with NSAMP = 12 (56 s integrations). Four images were taken in each broadband filter under a four-point square dither pattern, with 1.″9125 offsets on each side of the square. Offsets by nonintegral pixel sizes allow for better sampling of the PSF, and the four images in each filter were median combined on a 2 times resampled grid (0.″038 pixel^{-1}) after image reregistration. During the image registration/combination process, a +0.9% linear geometrical distortion (image $Y:X$) in NICMOS Camera 2 was corrected. The total target flux density was preserved in the resampling so that the flux density per pixel area is conserved.

The narrowband F215N and F216N images obtained as part of the van Der Welf GO program were not dithered. The narrowband images were taken with MIF512/NSAMP = 25 multiaccum sequences (integration time 512 s). Eight images were taken in the F216N filter (4096 s total integration time), while six images were taken in the F215N filter (3072 s total integration time). After each exposure, the telescope was chopped off the source by 90″ and sky background frames were taken in an identical manner. After recalibrating the raw frames (with postprocessing to interpolate and replace known bad pixels) to create count rate images, the sets of filtered target and background images were median combined.

The NICMOS narrowband F187N and F190N images were taken in GTO 7219 in the same spacecraft orbit as the broadband images (above) and under the same four-point dither pattern. At each dither point (for each filter) a single STEP8/NSAMP = 12 exposure (56 s integration) was taken, yielding 218 s total integration time after combining the four images. The data were processed in a manner similar to the broadband images. Measurements taking the pixel sampling into account yield a NICMOS Strehl ratio of ~98% in the F110W filter and the NIC2 camera used here.

5. RESULTS AND INTERPRETATION

5.1. *Broadband Imaging*

Figure 2*a* shows a false-color wide-field image of NGC 6240 and its guide star (on the left), from Keck AO. This image is 59″ wide by 47″ tall. Red corresponds to K' band, green to H band, and blue to J band. One can clearly see light from the extended parts of the galaxy in J band, with the characteristic "bow tie" shape known from previous work (e.g., Fig. 2 in Pasquali et al. 2003). The compact nuclear region is dominated by K'-band light; this is consistent with previous estimates of high dust extinction in the double nucleus (reviewed by Gerssen et al. 2004). Note that the guide star (*left*) is overexposed in this image and that it shows the sixfold symmetry expected from the Keck hexagonal pupil.

Figures 2*b* and 2*c* show false-color images of NGC 6240 over a slightly narrower field, 28.″5 × 33″. Here red represents the Keck K' AO image, green is F814W WFPC2 archival data from *HST*, and blue is F450W archival WFPC2 data. In these images spanning the wavelength range 450 nm to 2.1 μm, the highly structured dust lanes cutting through or in front of the central regions of NGC 6240 are clearly seen. Figure 2*b* has a linear color map; Figure 2*c* has a logarithmic color map so that the position of the double nucleus can be identified.

Figure 3 zooms in still further, showing the double nucleus of NGC 6240 in J, H, and K' bands from Keck AO (Figs. 3*a*, 3*b*, and 3*c*, respectively) and in F110W, F160W, and F222M from NICMOS (Figs. 3*d*, 3*e*, and 3*f*, respectively). North is up and east is to the left. The Keck images span 4.″2 in the north-south direction, corresponding to 1.9 kpc at the distance of NGC 6240; the NICMOS images are 3.″9 in the north-south direction, corresponding to 1.8 kpc.

Before we discuss the astrophysical content of these images, it is instructive to compare the technical performance of ground-based AO with that of NICMOS on *HST*. First and foremost, we

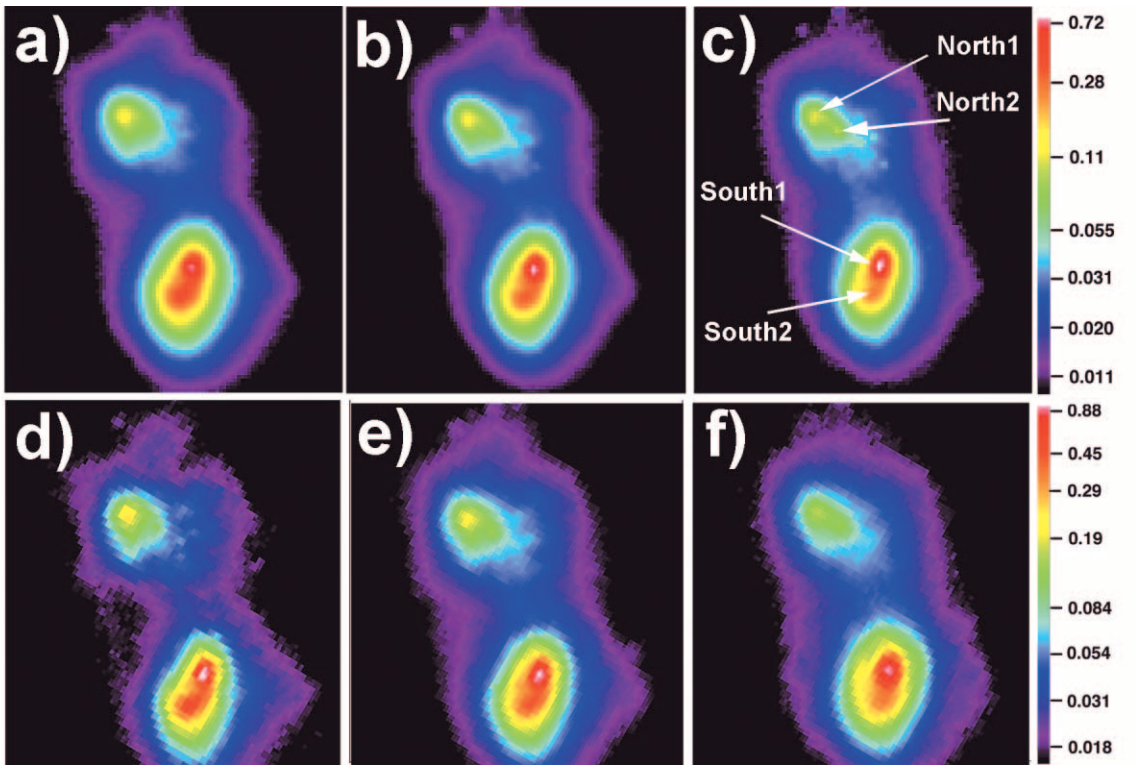

FIG. 3.—Double nucleus of NGC 6240. North is up and east is to the left. Top three panels show Keck AO images in (*a*) *J*, (*b*) *H*, and (*c*) *K*′ bands. Bottom three images show NICMOS images to approximately the same spatial scale: (*d*) F110W filter, (*e*) F160W filter, and (*f*) F222M filter. Keck images are ~4.″2 in the north-south (up-down) direction. NICMOS images shown here are ~3.″9 in the north-south direction. The color map is logarithmic. Each image has been rescaled so that the brightest pixel in its southern nucleus is white, in order to preserve dynamic range in the display. The two color bars shown for concreteness on the right of this figure correspond to panels (*c*) and (*f*).

note that all the major features of the two nuclei are seen in both Keck AO and NICMOS. This is distinctly reassuring, in view of the potential for AO images to contain artifacts due to imperfect calibration of non–common-path errors.

In terms of the more detailed substructures within each nucleus and between the two nuclei, the Keck AO and NICMOS images contain very complementary information. Close examination of the data at all three wavelengths indicates that the two main nuclei are surrounded by a multitude of unresolved pointlike sources. One can see from Figure 3 that these pointlike sources have highest contrast in the Keck *K*′ image (Fig. 3*c*) and in the NICMOS F110W (~*J*) image (Fig. 3*d*).

This qualitative impression from Figure 3 can be made more quantitative. Figure 4 shows images of one of the pointlike sources, located at $16^{h}52^{m}58^{s}.851$, +02°24′09.″75 (J2000.0), at three wavelengths with both Keck and NICMOS. The top row shows the Keck AO images with (*a*) *J* filter, (*b*) *H* filter, and (*c*) *K*′ filter. The bottom row shows the NICMOS images with (*d*) the F110W, (*e*) F160W, and (*f*) F222M filters. In each image, the dynamic range between black and white is a factor of 10 (actually 10 ± 1, owing to the vagaries of image reproduction). The compactness of the (black) core relative to the 10 times lower (white) background is a measure of the imaging performance. The numbers listed in Figure 4 and in Table 3 are the FWHM of the respective point-source images.

One sees from Figure 4 that for NICMOS the FWHM improves at shorter wavelengths, whereas for Keck AO the reverse is the case. This is because the imaging performance of a diffraction-limited telescope such as *HST* improves as the wavelength gets *shorter*, whereas the Strehl ratio for a given AO system improves as the wavelength gets *longer*. Both of these effects are seen in Figure 4, in which NICMOS has superior spatial resolution at F110W (*J* band) and Keck has better spatial resolution at *K* band.

In principle, one would expect a diffraction-limited Keck telescope, at 10 m diameter, to show more than 4 times better spatial resolution than NICMOS on *HST*. This increased spatial resolution is indeed achievable when (1) the guide star is bright (e.g., $V < 10$), (2) the guide star is close by (e.g., $<10''$), and (3) the pixel sampling used for the NIRC2 camera is appropriate for Nyquist sampling the diffraction limit at each wavelength. However, for the present observations none of these conditions were satisfied: the guide star was >13th magnitude, it was ~35″ away, and the 0.″04 pixels on NIRC2's wide camera do not Nyquist sample any of the *J*, *H*, and *K* wavelengths reported here.

A quantitative measure of point-source sensitivity comes from analyzing the signal-to-background ratio for the pointlike source shown in Figure 4, as well as for a second point source at $16^{h}52^{m}58^{s}.684$, +02°23′56.″9, J2000.0 (point source 2 in Table 3). Table 4 shows the signal-to-background ratios calculated for these two point sources for all three wavelength bands of Keck AO and NICMOS data. For both sources NICMOS has superior signal-to-background ratio at *J* and *H* bands, whereas Keck AO has superior signal-to-background ratio at *K* band/F222M.

We now return to the features seen in the two nuclei of NGC 6240 (Fig. 3). The most striking impression is that both the northern and southern nuclei are elongated, with considerable substructure within each nucleus. The brightest point in the northern nucleus is to the northeast. As shown in Figure 5, we refer to this as North1. The brightest point in the southern nucleus is to the north-northwest; we refer to this as South1. Just

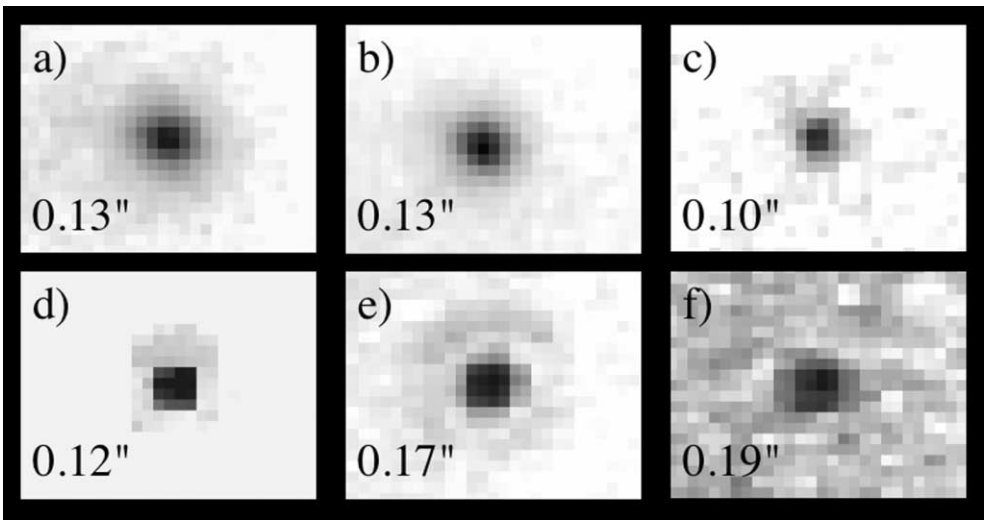

FIG. 4.—Images of a pointlike source located at $16^h52^m58^s.851, +02°24'09''.75$ (J2000.0) in three different wavelength bands. North is up and east is to the left. The top row shows the Keck AO images with (*a*) *J* filter, (*b*) *H* filter, and (*c*) *K′* filter. The bottom row shows the NICMOS images with (*d*) F110W, (*e*) F160W, and (*f*) F222M. These images are on a log gray scale. In each image, the dynamic range between black and white is a factor of 10 (actually 10 ± 1, owing to the vagaries of image reproduction). The compactness of the (black) core relative to the 10 times lower (white) background is a measure of the imaging performance. The numbers listed in the panels are the FWHM of the respective point-source images. The overall size of the Keck panels is ~1″.1 wide by 0″.8 tall. The NICMOS panels are ~1″.0 wide by 0″.8 tall.

outside the two nuclei are many unresolved pointlike sources that we propose are young star clusters, participating in the starburst in a manner similar to the clusters in the extranuclear regions of the NGC 6240 studied by Pasquali et al. (2003). Authors such as Zepf et al. (1999), Schweizer & Seitzer (1998), and Whitmore & Schweizer (1995) have shown in other spiral-galaxy mergers that pointlike sources analogous to these "have sizes, colors, and luminosities like those expected for young Galactic globular clusters." Figure 6 shows Keck AO *J*, *H*, and *K′* images of the nuclei of NGC 6240, with gray scale stretched so as to emphasize the pointlike sources just outside the two nuclei. The nature of the pointlike putative clusters in our images will be discussed in a future paper.

There are clear wavelength-dependent differences in morphology within both nuclei. First, consider the southern nucleus in Figure 3. In Keck *J* band (Fig. 3*a*) and NICMOS F110W (Fig. 3*d*) there are two clear intensity peaks within this nucleus, as there are at 814 nm (Gerssen et al. 2004; discussed further below). However, at longer wavelengths (*H* and *K′*) the primary peak, South1, becomes brighter relative to the secondary peak, which we call South2 (see Fig. 5). This can be seen more clearly in Figures 7*g* and 7*h*. From the Keck data using photometry with a 3 pixel radius aperture, the ratio of flux in South1 to flux in South2 is 1.23 at *J* band, 1.54 at *H* band, and 2.07 at *K′* band.

In the northern nucleus, Keck AO data in *K′* band show a new pointlike source emerging to the southwest of North1 (Figs. 7*d* and 5). This second point source is suggested in the NICMOS F222W image (Fig. 3*f*) but is more clearly differentiated in the Keck *K′* data. From the Keck data using photometry with a 3 pixel radius aperture, the ratio of flux in North2 to flux in North1 is 0.57 at *J* band, 0.60 at *H* band, and 0.68 at *K′* band. (In the *J*- and *H*-band photometry, we constrained the North2 aperture to be centered at the centroid of North2 at *K′* band.)

A three-color image synthesizing these data on the nuclear region is shown in Figure 8, which uses a square root color map. The NICMOS F110W image is shown in blue; the Keck *H* and *K′* images are in green and red, respectively. Light from the extended regions of the merging galaxies appears bluish in this image. Areas of high dust extinction appear selectively in red in Figure 8 and match those seen in Figures 2*b* and 2*c*.

The region of highest reddening extends north of the South1 nucleus, reaching into the gap between the northern and southern nuclei. In the CO map of Tacconi et al. (1999, their Fig. 1), the South1 nucleus lies at the southern edge of a region of high-density CO. Analogously, in our Keck data the South1 nucleus lies at the southern edge of a highly reddened region that we associate with Tacconi's CO cloud.

The most heavily reddened feature is the South1 nucleus, suggesting that it is the most deeply embedded in dust. We also note an "arm" of high reddening that wraps around the southern nucleus from northeast to southwest, separating the South1 and South2 subnuclei. This "arm" within the southern nuclear region has the appearance of a foreground dust lane, obscuring the bright regions behind it.

TABLE 3
FWHM FOR KECK ADAPTIVE OPTICS AND NICMOS IMAGES, FROM TWO POINTLIKE SOURCES

	J BAND		*H* BAND		*K* BAND	
PARAMETER	Point Source 1	Point Source 2	Point Source 1	Point Source 2	Point Source 1	Point Source 2
Keck FWHM (arcsec).....	0.13	0.16	0.13	0.13	0.10	0.12
NICMOS FWHM (arcsec).....	0.12	0.11	0.17	0.13	0.19	0.17

NOTES.—FWHM was measured using IDL's IMEXAM package as implemented in ATV. The fitting parameters were as follows: centering box radius = 7 pixels, inner sky radius = 10 pixels, outer sky radius = 20 pixels.

TABLE 4
Signal-to-Background Ratios for Keck AO and NICMOS Images of Two Pointlike Sources

	Point Source 1		Point Source 2	
Band/Filter	Keck AO	NICMOS	Keck AO	NICMOS
J/F110W	1.1	3.4	1.6	2.5
H/F160W	1.3	2.4	1.6	2.3
K′/F222M	2.6	0.7	3.6	0.9

Notes.—Object counts and sky counts were measured using IDL's IMEXAM package as implemented in ATV. The fitting parameters were as follows: centering box radius = 7 pixels, inner sky radius = 10 pixels, outer sky radius = 20 pixels. The aperture radius was chosen as that radius where the PSF has fallen to the sky background level as measured between radii of 10 and 20 pixels. Background counts were calculated by integrating IMEXAM's sky level out to the aperture radius.

5.2. *Differential Extinction toward the Two Nuclei and the Location of the Two AGNs*

Many authors have pointed out that the angular separation between the northern and southern nuclei is smaller at infrared wavelengths than in the visible. It is smaller still at millimeter and radio wavelengths. The angular separation measured by Gallimore & Beswick (2004) between the two brightest components was 1.″52 in their 5 GHz MERLIN radio data. The radio continuum properties of the two brightest nuclei seen in the 5 GHz MERLIN data resemble those of compact radio sources in Seyfert nuclei (including an inverted spectrum at low frequencies and high brightness temperatures). The distance between the two brightest MERLIN components is hence a good measure of the actual distance between the two black holes. Gerssen et al. (2004) measured the angular separation between the northern and southern nuclei as 1.″86 at *V* band and suggested that nonuniform dust obscuration of the southern nucleus, and possibly the northern nucleus as well, might explain the wavelength dependence of the angular separation.

We have shown our Keck AO data in *J* and *K′* band in Figure 7, along with archived WFPC2 data obtained by Gerssen et al. (2004) in the F450W filter (the so-called wide *B* filter, centered roughly where the *B* band is centered, but about twice as wide) and F814W filter (roughly Johnson *I* band). In the southern nucleus one sees the northwest component, which we have called South1 and which Gerssen et al. (2004) called N2, becoming more prominent relative to the southeastern component (our South2, and N1 in Gerssen et al. 2004) at longer wavelengths. The effect is quite striking: at F450W South1 is barely visible, whereas at *K′* band South1 is by far the more prominent subcomponent. This is consistent with the heavy reddening of South1 shown in Figure 8. In the northern nucleus, the southwestern component North2 is emerging as a pointlike source in *K′* band, whereas at F450W it is not visible at all.

There are two effects that make the angular separation between the northern and southern nuclei appear to be smaller at *K′* band than at F450W. At *K′* band, the photocentric location (i.e., the image centroid) of the southern nucleus is dominated by the contribution of the South1 source. At the same time, the emergence of North2 in *K′* band biases the photocentric location of the northern nucleus farther to the south than at shorter wavelengths. The measured separation between the centroids of the North1 and South1 subnuclei in the *HST* F450W filter is 1.″87. At *K′* band, where we begin to see the North2 subnucleus clearly, the separation between the North2 and South1 subcomponents is considerably smaller: 1.″59 ± 0.″02.

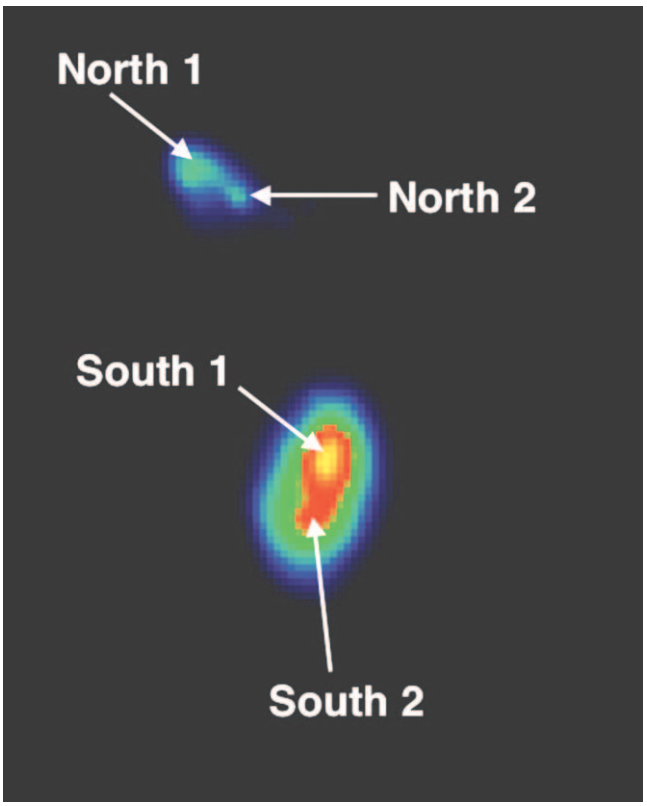

Fig. 5.—Positions of the northern and southern subnuclei referred to in the text from Keck *K′*-band data.

Thus, we conclude that the North2 and South1 nuclei are much more likely to be close to the two AGNs than the North1 and South 2 subnuclei that are so prominent in the F450W filter. However, because our 1.″59 *K′*-band separation between N2 and S1 is still not as small as the 1.″52 separation seen at 5 GHz, we agree with Gerssen et al. (2004) that even at *K′* band we are not completely penetrating the large amount of dust extinction: either one or both AGNs have not fully emerged from the dust in our *K′*-band images.

If the unresolved point source at North2 is the site of one of the black holes in NGC 6240, then the second black hole would lie north of South1 by about 0.″07, or approximately 2 pixels in the NIRC2 wide camera, based on the angular separation of 1.″52 between the two nonthermal radio sources at 5 GHz measured by Beswick.

5.3. *Narrowband Imaging in Lines of Molecular Hydrogen*

It has been known for more than 15 years that NGC 6240 has extended filamentary Hα emission over a region up to 50 kpc in size, which Heckman et al. (1987, 1990) interpreted as being due to a superwind driven by vigorous starburst activity. A recent paper by Veilleux et al. (2003) reinforces the interpretation that [N II] and Hα optical line emission from excited gas in NGC 6240 is associated with a superwind, presumably driven by the merger-induced starburst. NGC 6240 is also an extremely energetic emitter of near-infrared molecular hydrogen lines. With the high spatial resolution available via AO and NICMOS, one can use infrared narrowband imaging to gain insight into the spatial distribution of excited H_2 gas, to compare this with the spatial distributions of Hα and soft X-rays, and to integrate observations at these disparate wavelength bands into a more unified understanding of gas emission in starburst galaxies.

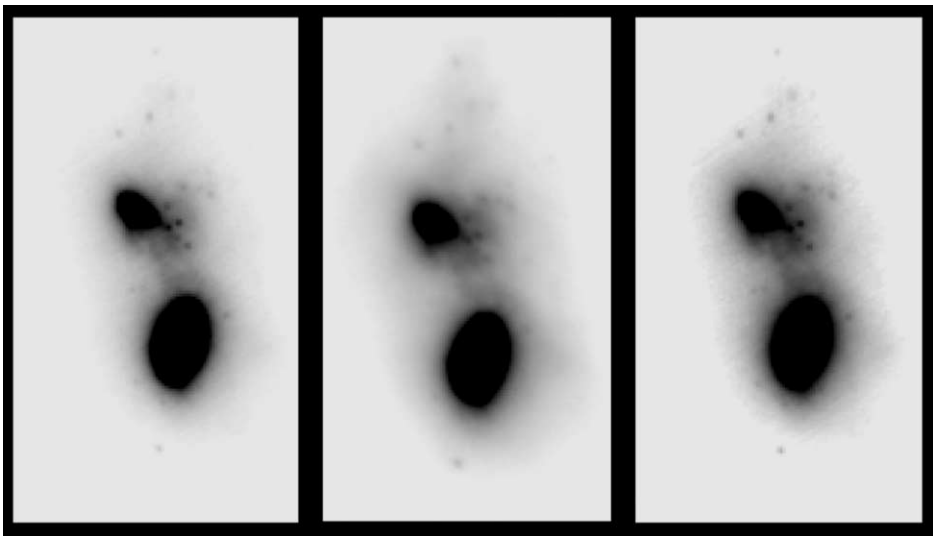

FIG. 6.—Keck AO images of the core of NGC 6240, using a gray-scale stretch that overexposes the nuclei and emphasizes the numerous pointlike sources in the nuclear region. *Left*: *J*-band image. *Middle*: *H*-band image. *Right*: K'-band image. These panels are 4.″2 wide by 7.″4 tall. North is up and east is to the left.

The physical processes that contribute to the complex spatial structure of molecular gas in NGC 6240 have been emerging over the past few years from observations with spatial resolution 0.″5–1″. Tacconi et al. (1999) reported observations with the IRAM millimeter-wave interferometer of the 1.3 mm CO $J = 2 \rightarrow 1$ line in the core of NGC 6240, at a spatial resolution of $0.''5 \times 0.''9$. Tacconi et al. (1999) interpreted their data as suggesting a rotating, turbulent thick molecular disk structure about 500 pc in diameter lying between the two nuclei (centered about 0.″6 north-northeast of the southern nucleus). Ohyama et al. (2000) used long-slit *K*-band spectroscopy with the Subaru telescope in seeing-limited mode and found a peak in H_2 1–0 $S(1)$ line emission between the two nuclei, but a bit closer to the southern nucleus (0.″4 north-northeast of the southern nucleus) than Tacconi's reported CO peak. In addition to the CO and H_2 structures between the two nuclei, a series of narrowband images by Sugai et al. (1997) and Herbst et al. (1990) under seeing-limited conditions and by Bogdanovic et al. (2003) with AO showed that there are diffuse extensions of the H_2 emission in directions southwest and southeast of the southern nucleus.

Because of the fortuitous redshift of NGC 6240 ($z = 0.0243$), the H_2 1–0 $S(1)$ emission line falls within the bandwidth of most standard narrowband Brγ filters. By imaging the H_2 1–0 $S(1)$ emission line in the nominal narrowband Brγ filter and subtracting the adjacent continuum in a narrowband filter centered at 2.124 μm, one can obtain images of NGC 6240 largely in light from the strong H_2 1–0 $S(1)$ emission line. Bogdanovic et al. (2003) used this type of narrowband imaging with the Lick Observatory AO system to delineate the structure of the extended H_2 emission regions southwest and southeast of the southern nucleus. We report here on analogous observations at higher spatial resolution and higher signal-to-noise ratio.

Figure 9 shows the continuum-subtracted H_2 images from Keck AO (Fig. 9*a*) and NICMOS on *HST* (Fig. 9*b*). The cross marks the position of the brightest pixel in broadband images of

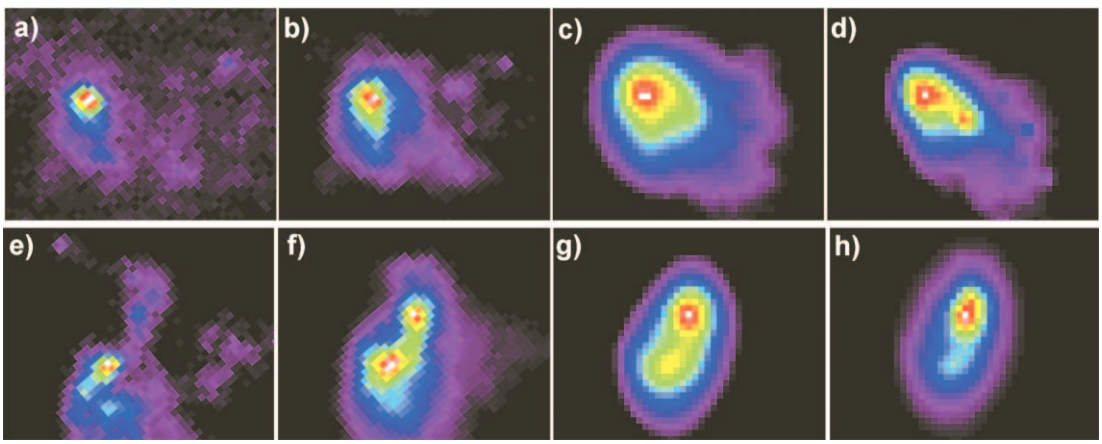

FIG. 7.—Spatially dependent extinction: features within the two nuclei of NGC 6240 as a function of observing wavelength; upper row shows northern nucleus, lower row shows southern nucleus. (*a*, *e*) *HST* WFPC2, F450W filter. (*b*, *f*) *HST* WFPC2, F814W filter. (*c*, *g*) Keck AO, *J* band. (*d*, *h*) Keck AO, K' band. This is a linear color map; each panel is rescaled so that the brightest pixel is shown in white. North is up and east is to the left. Panels (*a*–*d*) are 1.″7 wide by 1.″3 tall. Panels (*e*–*h*) are 1.″7 wide by 1.″5 tall.

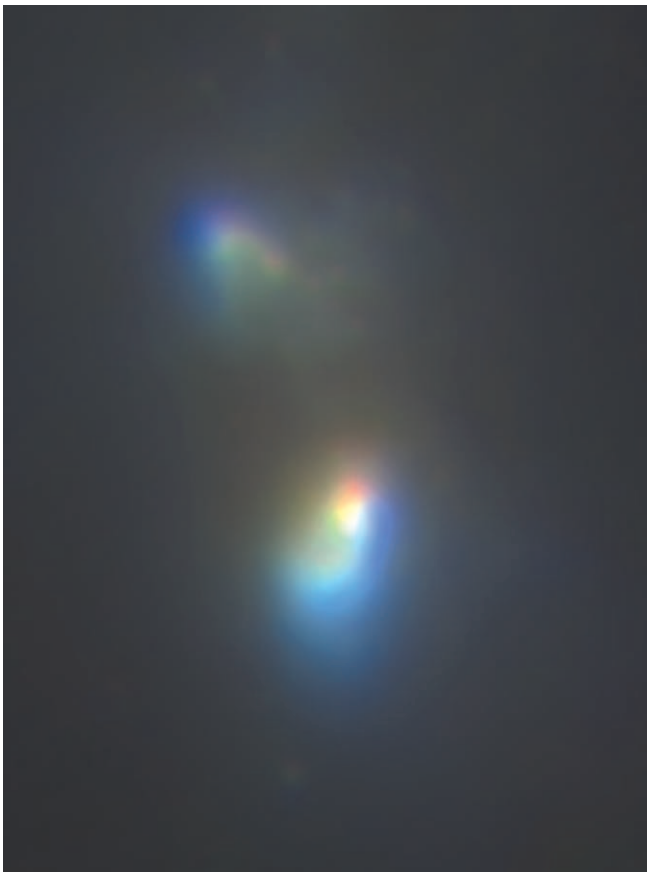

FIG. 8.—False-color F110W-*H*-*K*′ image of the nuclear regions of NGC 6240, using data from both NICMOS and Keck AO. This has a square root color map. The northern part of the South1 subnucleus is the most heavily reddened. North is up and east is to the left. This image is approximately 3.″8 wide by 5.″2 tall.

each of the two nuclei. Striking features of the H_2 emission include the following:

1. A "ribbon" of excited molecular hydrogen extending between the northern and southern nuclei. Figure 10 shows a zoomed-in section of Figure 9*a* highlighting the region between the two nuclei. The H_2 ribbon between the nuclei has a reverse S shape. It begins in a point source coincident with the southern nucleus (discussed below), departs the southern nucleus toward the east, and then curves in a long loop toward the northwest before turning east again to the northern nucleus. The Keck data show a hint that the "ribbon" may be subdivided into three separate "blobs." The H_2 "ribbon" occupies roughly the same region of projected sky as the peak of CO $J = 2 \rightarrow 1$ line emission noted by Tacconi et al. (1999) and Ohyama et al. (2003). For H_2, however, at the higher spatial resolution of Keck AO and NICMOS, the internuclear emission is oriented along a diagonal northwest-southeast line, in contrast to the north-south orientation of CO emission reported by Tacconi et al. (1999) at lower spatial resolution. Figure 11 shows the narrowband image from NICMOS in the H_2 1–0 $S(5)$ line (the difference between images in the F187N and F190N filters of NICMOS). Although the 1–0 $S(5)$ line is at lower signal-to-noise ratio than the 1–0 $S(1)$ line shown in Figures 9 and 10, the morphology of these two molecular hydrogen emission line images is quite similar; the 1–0 $S(5)$ line also shows a "ribbon-like" structure between the two nuclei.

The relation between the H_2 ribbon seen by Keck and NICMOS and the disk of dense CO and neutral hydrogen hypothesized by Tacconi et al. (1999) and Beswick et al. (2001) is not clear. Perhaps the diagonal ribbon is formed at the locations where flowing or expanding molecular hydrogen gas from the southern nucleus crashes into the outer layers of the Tacconi et al. (1999) north-south oriented cloud of CO lying between the two nuclei of NGC 6240.

However, an alternative explanation is also possible. Computer simulations (e.g., Barnes & Hernquist 1991, 1996) of disk

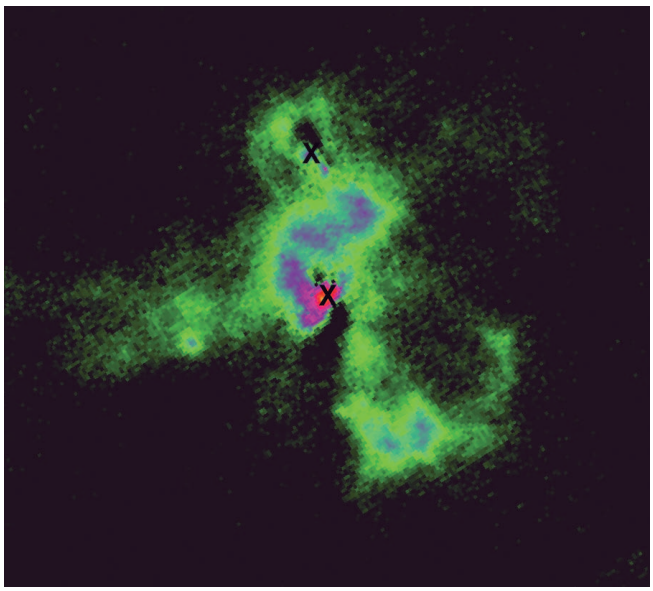

FIG. 9*a*

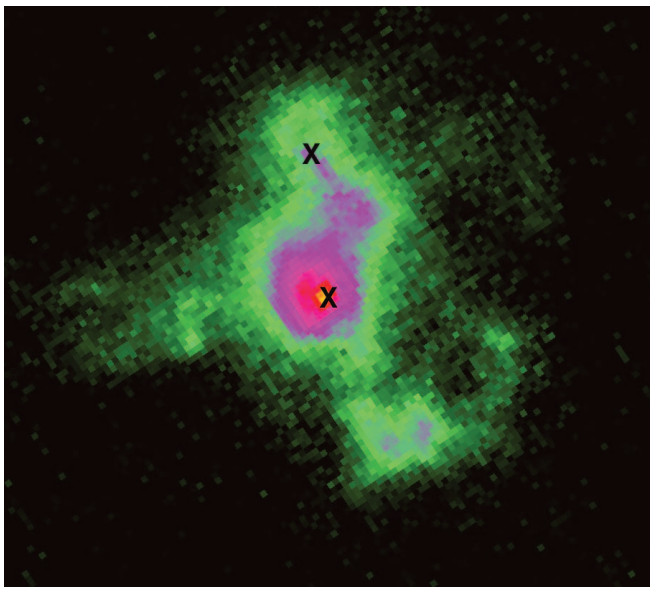

FIG. 9*b*

FIG. 9.—Narrowband images of the nuclear region of NGC 6240, in the H_2 1–0 $S(1)$ emission line. North is up and east is to the left. This has a log color map to emphasize fainter features. (*a*) Keck AO: dierence between images obtained in the Brγ filter and in the H_2 filter. White represents the peak flux, scaled to unity. Black represents fluxes <0.011 of the peak. This image is 7.″3 wide by 5.″8 tall. (*b*) NICMOS: difference between images obtained in F216N and F215N filters. White represents the peak flux, scaled to unity. Black represents fluxes <0.08 of the peak. This image is 7.″1 wide by 5.″1 tall. The two crosses mark the positions of the North1 and South1 nuclei as measured in continuum images.

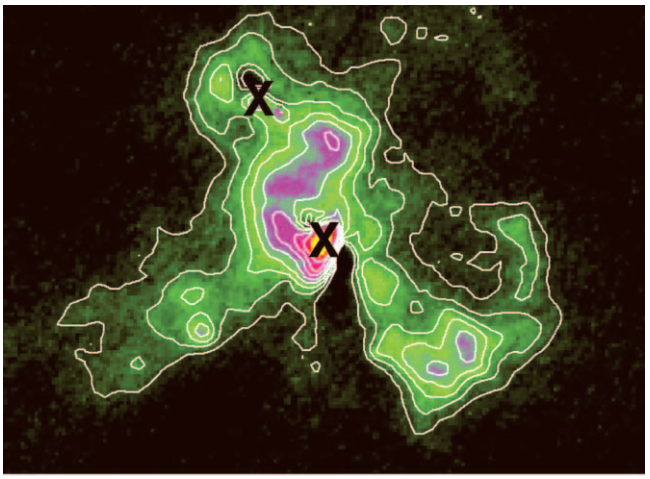

FIG. 10.—Keck AO narrowband image of the nuclear region in the H_2 1–0 $S(1)$ emission line (as in Fig. 9*a*), zoomed in so as to emphasize structures between and immediately around the two nuclei. This image is 7.″5 wide by 5.″5 tall and has a log color map. The eight contour levels are on a log scale, with the first contour at 0.2 times the maximum flux (at the South1 nucleus) and the last contour at 0.02 times the maximum flux. The black crosses show the position of the brightest pixels in the northern and southern nuclei, as seen on the unsubtracted image in the Brγ filter. These positions correspond to the North1 and South1 subnuclei. The North2 subnucleus also is bright in the difference image.

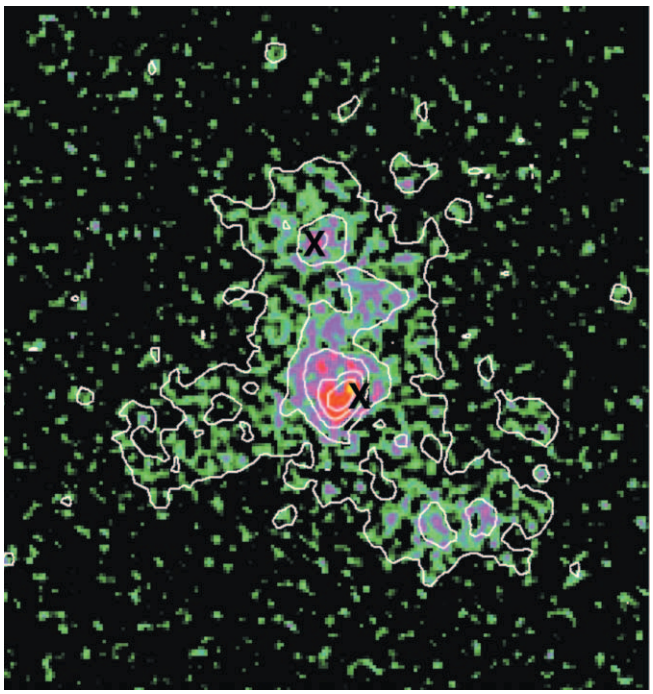

FIG. 11.—Narrowband NICMOS image of the core of NGC 6240 in the H_2 1–0 $S(5)$ line (difference between images in F187N and F190N filters). The image uses a log scale for the color map and contour lines and is geometrically corrected for the $Y : X = 0.9\%$ linear geometrical distortion in NICMOS Camera 2. Although the 1–0 $S(5)$ line is at lower signal-to-noise ratio than the 1–0 $S(1)$ line shown in Fig. 9, the morphology of these two molecular hydrogen emission line images is quite similar. This image is 8″ wide by 8.″2 tall.

galaxy mergers show that "a significant amount of material flows along the bridge connecting the galaxies. . . ." (Barnes & Hernquist 1991; see also Figs. 9 and 10 in Barnes & Hernquist 1996; Figs. 1 and 4 in Barnes 2002). The morphology of the H_2 ribbon seen by Keck and NICMOS suggests that we may indeed be seeing gas flowing from one nucleus to the other, with an elongated and irregular shape determined by both the initial parameters of the galaxy merger and tidal distortion of the "bridge" between the two galaxies. Future spatially resolved AO spectroscopy will help to assess these varying hypotheses.

2. Compact knots of H_2 emission to the northeast of the northern nucleus, to the east-southeast of the southern nucleus, and to the south-southwest of the southern nucleus. Each of these compact knots corresponds to one of the CO features noted by Tacconi et al. (1999) as D, C, and A in their Figure 1 and was noted by Bogdanovic et al. (2003) in Lick AO data. These features were shown by Tacconi et al. (1999) to have distinct CO velocity structure; hence, they are presumably distinct dynamical entities. A plausible hypothesis is that these are star-forming or starburst regions, a hypothesis that can be tested via future AO spectroscopy of each knot.

3. Pointlike H_2 emission at the southern nucleus. Figure 9 shows that in both the Keck AO and NICMOS images we see pointlike H_2 emission at the position of the southern nucleus (South1). We measured the centroid of the bright point corresponding to the South1 subnucleus in the continuum-subtracted H_2 image and compared it with the centroid of South1 in the continuum image. For the Keck AO data, these positions were identical to within less than a pixel ($<0.''04$), consistent with the measurement error. These data are consistent with the hypothesis that the positions of the peak H_2 emission and of the peak continuum emission are coincident to within the diffraction limit of the telescope. We did the same exercise for the H_2 emission from the North1 and North2 nuclei, evident in Figure 10. As for the South1 subnucleus, the peak H_2 emission from North1 and North2 corresponded in position to that in the continuum image.

Using seeing-limited observations, previous authors (Tecza et al. 2000; Herbst et al. 1990; van der Werf et al. 1993; Sugai et al. 1997; Ohyama et al. 2000) have reported that the peak of the H_2 is displaced $0.''35$–$0.''4$ north of the southern nucleus, in the direction of the northern nucleus. Our high-resolution data from both Keck AO and NICMOS are not consistent with this displacement. We point out that the complex ribbon-like spatial structure of the H_2 emission seen in Figures 9 and 10 might cause a seeing-limited image to have a centroid that is displaced northward of the southern nucleus.

4. Filamentary structure in molecular hydrogen. In the region *exterior* to the two nuclei of NGC 6240, the filaments of excited H_2 observed by Keck AO and NICMOS correspond well to the filaments observed in Hα emission by WFPC2 on *HST*. This can be seen in the contour plots of H_2 and Hα shown in Figures 12*a* and 12*b*, respectively. Referring to the *Chandra* observations of Komossa et al. (2003), shown as a contour plot in Figure 13, the two largest H_2 and Hα filamentary loops in Figure 12 to the east and west of the northern nucleus trace the exterior boundaries of two "bubbles" of soft X-ray emission observed by *Chandra*. The Hα emission around the circumference of these bubbles (Fig. 12*b*) persists to larger distance from the center of the nuclear region than does the H_2 emission (Fig. 12*a*), possibly indicating that the molecular clouds are more concentrated in the nuclear region. Komossa et al. (2003) suggest that the extended soft X-ray "bubble" features are filled with hot ($kT = 0.8$–2.8 keV) low-density (0.1 particle cm^{-3}) gas and are powered by starburst-driven superwinds with mechanical input power from roughly three supernovae per year over a starburst duration of 3×10^7 yr. In this scenario the H_2 and Hα line emission shown in Figure 12 would come from a thin layer around

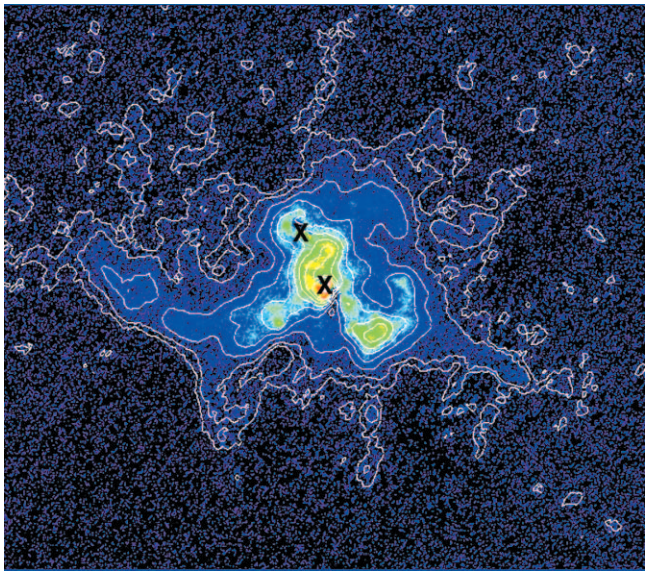

FIG. 12*a*

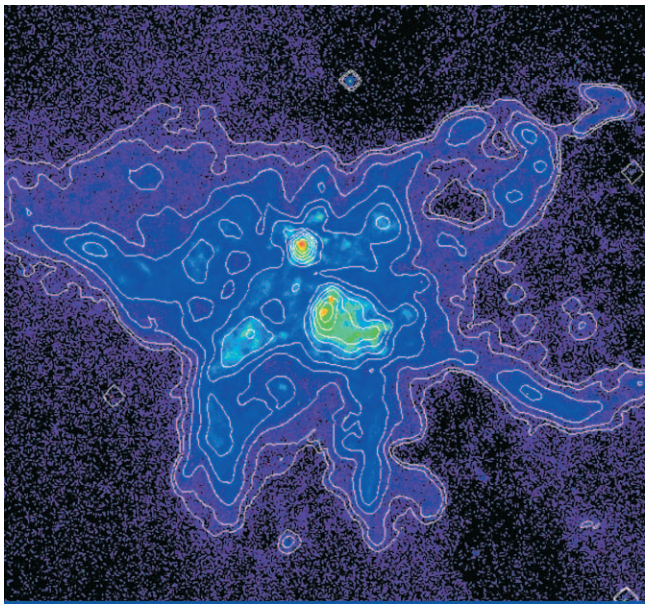

FIG. 12*b*

FIG. 12.—Contour plots of line-emitting gas in the region outside the two nuclei of NGC 6240. This has a square root color map and contour scale to emphasize fainter structures. (*a*) H_2 1–0 $S(1)$ emission line from Keck AO. (*b*) Hα emission from the WFPC2 camera on *HST* (F673N filter, archival data from *HST* proposal number 6430, PI: van der Marel). Panel (*a*) is 20.″2 wide by 16.″4 tall; panel (*b*) is 19.″6 wide by 16.″3 tall.

the edges of these extended soft X-ray bubbles, in locations where the starburst wind is driving shocks or ionization fronts into the interstellar medium and surrounding molecular clouds.

6. CONCLUSIONS

We have presented results of near-infrared imaging of NGC 6240 using AO on the Keck II Telescope and NICMOS on *HST*. Broadband Keck images were obtained in J, H, and K' bands. NICMOS images were in filters approximately corresponding to those at Keck. In addition, narrowband images were obtained in the 1–0 $S(1)$ and the 1–0 $S(5)$ emission lines of molecular hydrogen.

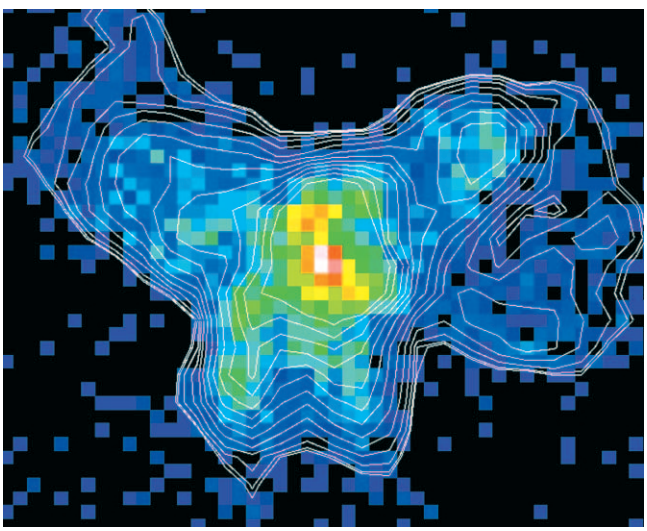

FIG. 13.—Contour plot of 0.5–8 keV X-ray emission from NGC 6240, from archived *Chandra* ACIS-S data of Komossa et al. (2003). Exposure time was 27 ks. This has a square root color map and contours, to emphasize fainter features. The image is 20.″2 wide by 16.″7 tall.

In general, we find very good agreement between the Keck AO and NICMOS data. The Keck AO images have somewhat higher spatial resolution in K band, whereas NICMOS is superior in F110W (roughly analogous to J band). On this basis we foresee continued strong synergy between ground-based AO on 8–10 m telescopes and space-based near-infrared observations on somewhat smaller telescopes.

Both the northern and southern nuclei of NGC 6240 are clearly elongated, with considerable substructure within each nucleus. In K' band there are at least two point sources within the northern nucleus; we tentatively identify the southwestern point source as the position of one of the two AGNs. In the southern nucleus, the northern subnucleus is the most highly reddened. Using the nuclear separation measured in the radio at 5 GHz, we suggest that the AGN in the southern nucleus is still enshrouded in dust at K' band and is located approximately 0.″07 to the north of the K'-band position of the northern subnucleus.

Within the southern nucleus there is strong pointlike H_2 1–0 $S(1)$ line emission from the northern subnucleus, contrary to the conclusions of previous seeing-limited observations. Narrowband H_2 emission line images show that a streamer or ribbon of excited molecular hydrogen connects the northern and southern nuclei, on a diagonal from southeast to northwest. We suggest that this linear feature corresponds to a bridge of gas connecting the two nuclei (and perhaps flowing between them), as seen in computer simulations of mergers. The connection between this streamer and the "disk" of CO seen at lower spatial resolution by previous observers is not yet clear.

Finally, many pointlike regions are seen around the two nuclei. These are most prominent in J band with NICMOS and in K' band with Keck AO. We suggest that these point sources represent star clusters formed in the course of the merger. In future observations it will be of great interest to determine the ages of these star clusters and to determine what fraction of NGC 6240's starburst activity can be attributed to them.

We enthusiastically thank the staff of the W. M. Keck Observatory, and especially David Le Mignant and the other members of its AO team, for their dedication and hard work. Data presented herein were obtained at the W. M. Keck Observatory, which is operated as a scientific partnership among the California Institute of Technology, the University of California, and the National Aeronautics and Space Administration. The Observatory and the Keck II AO system were both made possible by the generous financial support of the W. M. Keck Foundation. The authors wish to extend special thanks to those of Hawaiian ancestry on whose sacred mountain we are privileged to be guests. Without their generous hospitality, the observations presented herein would not have been possible.

This work was supported in part under the auspices of the US Department of Energy, National Nuclear Security Administration by the University of California, Lawrence Livermore National Laboratory under contract W-7405-Eng-48. This work was supported in part by the National Science Foundation Science and Technology Center for Adaptive Optics, managed by the University of California at Santa Cruz under cooperative agreement AST 98-76783. D. W. and R. A. acknowledge a minigrant from the Institute of Geophysics and Planetary Physics at the Lawrence Livermore National Laboratory. The work by R. A. was supported in part by NSF grant AST 00-98719. The NICMOS observations reported herein were obtained with the NASA/ESA *Hubble Space Telescope* operated by the Space Telescope Science Institute managed by the Association of Universities for Research in Astronomy, Inc., under NASA contract NAS5-26555. This work was also supported in part by NASA grants NAG 5-3042 and NAS 2-26555 to the NICMOS IDT.

REFERENCES

Armus, L., Heckman, T. M., & Miley, G. K. 1990, ApJ, 364, 471
Barnes, J. E. 2002, MNRAS, 333, 481
Barnes, J. E., & Hernquist, L. E. 1991, ApJ, 370, L65
———. 1996, ApJ, 471, 115
Beswick, R. J., Pedlar, A., Mundell, C. G., & Gallimore, J. F. 2001, MNRAS, 325, 151
Bogdanovic, T., Ge, J., Max, C. E., & Raschke, L. M. 2003, AJ, 126, 2299
Canalizo, G., & Stockton, A. 2001, ApJ, 555, 719
Fosbury, R. A. E., & Wall, J. V. 1979, MNRAS, 189, 79
Gallimore, J. F., & Beswick, R. 2004, AJ, 127, 239
Genzel, R., et al. 1998, ApJ, 498, 579
Gerssen, J., van der Marel, R. P., Axon, D., Mihos, C., Hernquist, L., & Barnes, J. E. 2001, in ASP Conf. Ser. 249, The Central Kiloparsec of Starbursts and AGN: The La Palma Connection, ed. J. H. Knapen et al. (San Francisco: ASP), 665
———. 2004, AJ, 127, 75
Heckman, T. M., Armus, L., & Miley, G. K. 1987, AJ, 93, 276
———. 1990, ApJS, 74, 833
Herbst, T. M., Graham, J. R., Beckwith, S., Tsutsui, K., Soifer, B. T., & Matthews, K. 1990, AJ, 99, 1773
Iwasawa, K., & Comastri, A. 1998, MNRAS, 297, 1219
Johansson, E. M., et al. 2000, Proc. SPIE, 4007, 600
Joseph, R. D., Wade, R., & Wright, G. S. 1984, Nature, 311, 132
Kennicutt, R. C., Jr., & Keel, W. C. 1984, ApJ, 279, L5
Komossa, S., Burwitz, V., Hasinger, G., Predehl, P., Kaastra, J., & Ikebe, Y. 2003, ApJ, 582, L15
Lutz, D., Sturm, E., Genzel, R., Spoon, H. W. W., Moorwood, A. F. M., Netzer, H., & Sternberg, A. 2003, A&A, 409, 867
Norman, C., & Scoville, N. 1988, ApJ, 332, 124
Ohyama, Y., Yoshida, M., & Takata, T. 2003, AJ, 126, 2291
Ohyama, Y., et al. 2000, PASJ, 52, 563
Pasquali, A., de Grijs, R., & Gallagher, J. S. 2003, MNRAS, 345, 161
Rafanelli, P., Schulz, H., Barbieri, C., Komossa, S., Mebold, U., Baruffolo, A., & Radovich, M. 1997, A&A, 327, 901
Roye, E., et al. 2003, NICMOS Instrument Handbook, Version 6.1 (Baltimore: STScI)
Sanders, D. B., & Mirabel, I. F. 1996, ARA&A, 34, 749
Schweizer, F., & Seitzer, P. 1998, AJ, 116, 2206
Scoville, N., et al. 2000, AJ, 119, 991
Sugai, H., Malkan, M. A., Ward, M. J., Davies, R. I., & McLean, I. S. 1997, ApJ, 481, 186
Tacconi, L. J., Genzel, R., Tecza, M., Gallimore, J. F., Downes, D., & Scoville, N. Z. 1999, ApJ, 524, 732
Tecza, M., Genzel, R., Tacconi, L. J., Andres, S., Tacconi-Garman, L. E., & Thatte, N. 2000, ApJ, 537, 178
Thompson, R. I., Rieke, M., Schneider, G., Hines, D. C., & Corbin, M. R. 1998, ApJ, 492, L95
Toomre, A., & Toomre, J. 1972, ApJ, 178, 623
van der Werf, P. P., Genzel, R., Krabbe, A., Blietz, M., Lutz, D., Drapatz, S., Ward, M. J., & Forbes, D. A. 1993, ApJ, 405, 522
Veilleux, S., Kim, D.-C., Sanders, D. B., Mazzarella, J. M., & Soifer, B. T. 1995, ApJS, 98, 171
Veilleux, S., Shopbell, P. L., Rupke, D. S., Bland-Hawthorn, J., & Cecil, G. 2003, AJ, 126, 2185
Véran, J.-P., Rigaut, F., Maître, H., & Rouan, D. 1997, J. Opt. Soc. Am. A, 14, 3057
Vignati, P., et al. 1999, A&A, 349, L57
Whitmore, B. C., & Schweizer, F. 1995, AJ, 109, 960
Wizinowich, P. L., Acton, D. S., Lai, O., Gathright, J., Lupton, W., & Stomski, P. J. 2000a, Proc. SPIE, 4007, 2
Wizinowich, P. L., et al. 2000b, PASP, 112, 315
Wright, G. S., Joseph, R. D., & Meikle, W. P. S. 1984, Nature, 309, 430
Zepf, S. E., Ashman, K. M., English, J., Freeman, K. C., & Sharples, R. M. 1999, AJ, 118, 752